Hydrogen Fuel Cell and Battery Hybrid Architecture for Range Extension of Electric VTOL (eVTOL) Aircraft

Wanyi Ng*
Graduate Research Assistant
University of Maryland
College Park, MD

Mrinalgouda Patil
Graduate Research Assistant
University of Maryland
College Park, MD USA

Anubhav Datta†
Associate Professor
University of Maryland
College Park, MD

The objective of this paper is to study the impact of combining hydrogen fuel cells with lithium-ion batteries through an ideal power-sharing architecture to mitigate the poor range and endurance of battery powered electric vertical takeoff and landing (eVTOL) aircraft. The benefits of combining the two sources is first illustrated by a conceptual sizing of an electric tiltrotor for an urban air taxi mission of 75 mi cruise and 5 min hover. It is shown that an aircraft of 5000–6000 lb gross weight can carry a practical payload of 500 lb (two to three seats) with present levels of battery specific energy (150 Wh/kg) if only a battery–fuel cell hybrid power plant is used, combined in an ideal power-sharing manner, as long as high burst C-rate batteries are available (4–10 C). A power plant using batteries alone can carry less than half the payload; use of fuel cells alone cannot lift off the ground. Next, the operation of such a system is demonstrated using systematic hardware testing. The concepts of unregulated and regulated power-sharing architectures are described. A regulated architecture that can implement ideal power sharing is built up in a step-by-step manner. It is found only two switches and three DC-to-DC converters are necessary, and if placed appropriately, are sufficient to achieve the desired power flow. Finally, a simple power system model is developed, validated with test data and used to gain fundamental understanding of power sharing.

Nomenclature

C	battery capacity, ampere hour, Ah
I	load current, ampere, A
i_b	battery current, A
i_c	current at output terminal of DC–DC converter, A
i_f	fuel cell current, A
P_b	battery power, watt (W)
P_f	fuel cell stack power, W
R_b	combined resistance of wires and diode in battery branch, ohm (Ω)
R_f	combined resistance of wires and diode in fuel cell stack branch, Ω
soc	battery state of charge
V	load voltage, volt (V)
V_b	battery voltage, V
V_c	voltage at output terminal of DC–DC converter, V
V_f	fuel cell stack voltage, V
W_f	weight of hydrogen ÷ weight of tank system including hydrogen, in %
α	fraction of battery power to total power supplied
β	efficiency of DC–DC converter
κ	ratio of load power to the total power generated

Introduction

Recent advances in electrochemical power and permanent magnet motors have generated a significant resurgence of interest in manned electric vertical takeoff and landing (eVTOL) aircraft (Refs. 1, 2). An eVTOL is defined as a vertical lift aircraft propelled by electric power and capable of carrying people. Since the first electric manned helicopter flights in 2011 (Ref. 3) and 2012 (Ref. 4), developers ranging from start-ups to major aerospace corporations have introduced many eVTOL concepts that are at various stages of development. Electric power offers the promise of cleaner, quieter, safer, and more agile aircraft, which are the desirable attributes of a new urban air mobility system. Cleanliness results from the lack of particulate pollution from the aircraft, often in densely populated areas, as well as the potential for the use of renewable energy for charging batteries or powering water electrolysis to produce hydrogen. Quietness results from a combination of reduced engine noise and slowed tip speeds enabled by electric motors, and aircraft optimized for primarily forward flight missions. Safety results from redundancy in distributed rotors and multiple power sources. Agility results from the ability to quickly vary rotor RPM and the increased thrust moment in distributed propulsion. Distributed propulsion, or the inclusion of many rotors distributed throughout the aircraft, is enabled by electric power; the drivetrain is changed from mechanical shafts to electrical wires. In 2017, Uber released a vision for an urban air mobility system in a white

*Currently Aerospace Engineer, NASA Goddard Space Flight Center.
†Corresponding author; email: datta@umd.edu.
Presented at the Vertical Flight Society 75th Annual Forum & Technology Display, Philadelphia, PA, May 13–16, 2019. Manuscript received September 2019; accepted October 2020.

paper (Ref. 5). The principal drawback of these electric aircraft is the poor range and endurance with practical payload (at least two to four passengers). This drawback stems from the specific energy of lithium-ion (Li-ion) batteries.

A major limitation for battery-powered eVTOL is the specific energy of Li-ion batteries—a maximum of 250 Wh/kg for cells (based on Panasonic cells) and 150–170 Wh/kg for packs (based on Tesla and Saft batteries) at beginning of life. High specific power (fast discharge) cells have even lower specific energy around 150 Wh/kg. Batteries also have long charging times. Proton exchange membrane (PEM) fuel cells using hydrogen fuel is an alternative that can offer significantly higher specific energy than batteries, in a unit that is still clean and hydrocarbon free, mechanically simple, operates at low temperatures (80–100 °C) and produces no harmful emissions during flight. In contrast to batteries, the specific energy of hydrogen fuel is 39.4 kWh/kg with an efficiency of around 0.45 when used in fuel cells. This is much higher even than the specific energy of gasoline, 13 kWh/kg with an efficiency of 0.3 (Carnot efficiency). However, the low-weight efficiency of hydrogen storage diminishes the advantage. The state-of-the-art hydrogen storage weight fraction is 5.5%, so the specific energy of hydrogen including storage is reduced to $39.4 \times 0.45 \times 0.055 = 1$ kWh/kg. This is still four times higher than the battery-specific energy. The key limitation of fuel cells is low specific power, perhaps around 0.5 kW/kg at best (based on Protonex Ion Tiger and HES A-1000 stacks). So the requirement to hover produces a very heavy stack. A combination of the high specific power of batteries with the high specific energy of fuel cells can reduce the total power plant weight, allow fast charging and refueling, and introduce redundancy in the power source for added safety.

Traditionally, fuel cells suffer from two major drawbacks, but the operating environment of eVTOL might make them less detrimental. First, fuel cells have poor low-pressure performance, so at very high altitudes a heavy compressor would be needed. But for low-altitude urban flights, unpressurized stacks would be adequate. Second, hydrogen typically requires a heavy tank to prevent boil-off over long periods of storage. But eVTOL would require only a few hours of storage at most, so the tank weight can be significantly reduced. An unavoidable downside of hydrogen fuel cells is the higher cost, at least initially, due to an expensive platinum catalyst, and the requirement of a new fuel infrastructure. Lithium-ion also has strategic challenges, such as the availability of cobalt and even graphite, but these factors are considered outside the scope of this paper.

Fuel cell and battery hybrid systems have been demonstrated in all-electric manned fixed-wing aircraft. The Boeing Fuel Cell Demonstrator achieved manned flight in 2008 with a gross weight of 870 kg for approximately 45 min (Ref. 6). The German Aerospace Center's electric motor glider Antares DLR-H2 has been successfully used as a flying test bed with a gross takeoff weight of 825 kg (Refs. 7–9). This aircraft has been used to investigate different hybridization architectures and methods to increase reliability. The ENFICA-FC project at Politecnico di Torino developed a two-seater hybrid aircraft that achieved an endurance of 40 min (Ref. 10). These aircraft serve as a proof of concept for fuel cell–powered flight, provide flight data, and identify key obstacles compared to conventional aircraft.

However, all of the above are fixed-wing aircraft. An eVTOL is a rotary-wing aircraft, which has unique challenges associated with high hover power, low lift-to-drag ratios (due to the edgewise rotor and hub drag), and highly transient power profiles, including high power both during takeoff and landing. Thus hybridization requires far more precise control of power sharing, and if achieved, promises greater pay off than airplanes. The intent of this paper is to demonstrate this capability.

Recently, special-purpose rotary-wing drones have also been flown using fuel cells. These are small-scale aircraft, and scarce data are available in the public domain. These aircraft include the United Technologies Research Center's 1.75 kW, 10 kg, single main rotor helicopter in 2009 (Ref. 11) and EnergyOr's 1.5 kW, 9.5 kg quadcopter in 2015 (Ref. 12). It is not clear what types of power architecture were included in these vehicles.

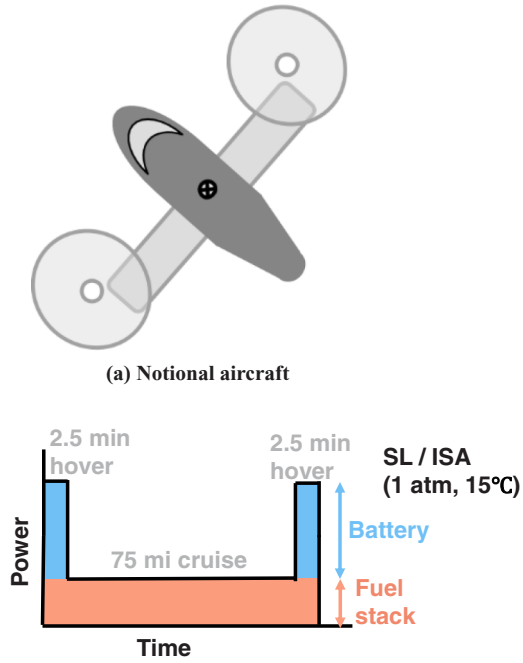

(a) Notional aircraft

(b) Notional mission power profile

Fig. 1. Notional aircraft and mission used for sizing analysis: (a) diagram of a two-rotor tiltrotor concept; (b) baseline power profile used, showing a B–FC hybrid power sharing scheme.

eVTOL Sizing with Fuel Cell

The potential benefits of battery–fuel cell (B–FC) hybridization were illustrated through a paper conversion of a piston-powered R-22 Beta II-like helicopter in Refs. 13 and 14. This preliminary study was significantly expanded in Ref. 15 by using weight models from actual hardware and applied to size a generic tiltrotor. This study further established the benefits of hybridization and motivated the present work. The present work was originally published as a conference paper (Ref. 16). This paper summarizes the final results. A summary of eVTOL sizing with fuel cell published in Refs. 15 and 16 is presented in this section for completeness. Some of the structural weight models are refined.

Figures 1(a) and 1(b) show notional diagrams of the configuration and mission, respectively. The mission is 5 min hover at 500 kW and 75 miles of cruise at the best range speed. Gross takeoff weight and payload are unknowns. As in Ref. 15, payload here includes fixed useful weights, such as the pilot and crew. Baseline conditions are SL/ISA (Sea Level/International Standard Atmosphere) with excursions up to 5000 ft/ISA + 20 °C. An elementary mission suffices for a new power plant so that principal trends are not buried under the details of start-up, shutdown, reserves, etc.

Figures 2 and 3 summarize the impact of power plant design on the weights. The results presented here are slightly refined from Refs. 15 and 16. Earlier, a constant structural weight fraction was used, whereas here, detailed weights corresponding to SAWE (Society of Allied Weight Engineers) standards consistent with NDARC (NASA Design and Analysis

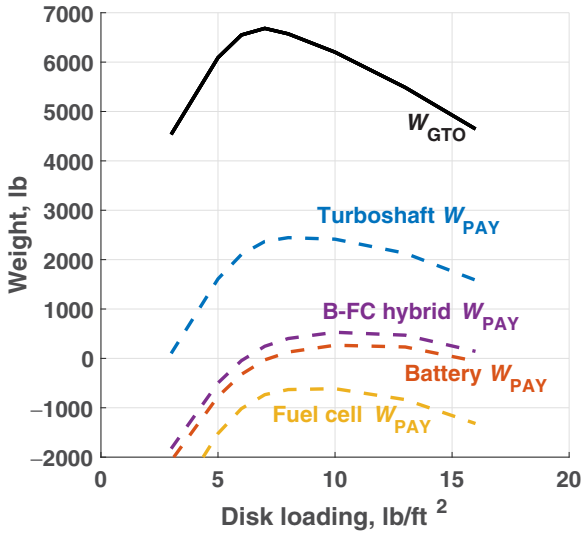

Fig. 2. Payload with various power sources using baseline technologies for a mission with 5 min hover at 500 kW and 75 miles of cruise at the best range speed.

of Rotorcraft) (Ref. 17) are used. The NDARC relations were calibrated with XV-15 data obtained from Ames Research Center, and the resulting calibration factors are shown in Table 1. The direct drive motor is also replaced with a gearbox. The motor is assumed to operate at a maximum speed of 8000 revolutions per minute (rpm) in hover when the rotor tip Mach number is 0.55. Figure 4 shows the variation of motor and gearbox weights with gear ratio. Operating at a higher gear ratio produces a lighter drive. The gearbox may also shield the motor from rotor vibratory loads. The overall performance of the aircraft and the general trends of results remain same as that of Refs. 15 and 16.

Figure 2 shows the gross takeoff weights and payload weights for a turboshaft, fuel cell, battery, and B–FC hybrid power plant. The electric power plant takes advantage of the electric motor to reduce cruise tip Mach number to 0.28 and achieve aircraft *L*/*D* of around 9–9.2 (see Ref. 15 for details). The sizing results use conservative baseline technologies for the electric power components. This includes a battery available specific energy of 150 Wh/kg (based on Tesla and Saft battery packs), a fuel cell stack specific power of 0.5 kW/kg (based on Protonex Ion Tiger and HES A-1000, but far lower than what reported by Honda and Toyota), and a hydrogen storage weight fraction of 5.4% (Department of Energy's already met Year 2015 target with stringent boil-off restrictions). The specific powers of fuel cell stacks can easily range from 0.1 kW/kg for inexpensive laboratory grade stacks to 2.0 kW/kg for expensive automobile stacks. There is also a general lack of well-defined archival data. Figure 5 compiles what is available in public. The automobile data are well archived in Refs. 18–20. Most of the data are from commercial vendors; some include balance of plant some do not; some quote rated power some maximum; some include ancillary equipment some do not; some are liquid cooled some air cooled. Among the UAV stacks, only the United Technologies helicopter and Navy Ion Tiger fixed-wing aircraft have weights well documented. Some others include even the hydrogen storage system. A power-to-weight ratio of 0.5 kW/kg is chosen as a reasonable average. These numbers ultimately resulted in a specific energy of 0.96 kWh/kg. A 15% overhead in weight and a 20% overhead in power are assumed, based on a small-scale hardware test. The power overhead includes cooling. For large aircraft, there might be additional cooling drag (perhaps up to 10–15% of the baseline fuselage drag in airplanes), but a realistic assessment requires far greater details than the drag model used here. The assumption here is that the overall drag remains calibrated to XV-15 flight-test data as validated in Ref. 15.

The battery is assumed to be energy limited rather than power limited, and sized according to its specific energy. The C-rate ζ is then a fallout. The hybrid power plant includes a fuel cell stack sized to accommodate the cruise power, and a battery sized to accommodate the additional boost required in hover. Charging the battery during the mission—a special feature of the architecture given later in this paper was not considered. It is demonstrated later that charging, if incorporated, and applicable to the mission, can only improve the payload. The results, without charging, show that only the B–FC hybrid power plant can carry a practical payload. For a gross takeoff weight of 6200 lb, the payload is around 550 lb at a disk loading of 10 lb/ft^2. Fuel cells that provide 0.5 kW/kg specific power still require a custom design. The batteries consist of 150 Wh/kg installed and available with at least 6C continuous during 5 min of hover: 68 units of nine cells and each cell is rated at (10 C) 100 Ah. These are high-power cells and will also require custom design.

Figure 3 shows several design excursions. Figure 3(a) shows the effects of improvements in fuel cell and hydrogen storage technology. A 7.5% weight fraction is a reasonable value to use in aviation, where boil-off is of lesser concern than in automobiles because of shorter storage time (hours compared to days). This weight fraction results in an increased specific energy, of the fuel and tank combined, of 1.32 kWh/kg. Increasing the specific power of a fuel cell stack to Honda and Toyota's reported 2 kW/kg (Refs. 18–20) decreases the weight significantly to the point where a fuel cell power plant can accommodate a useful payload of around 1800 lb at a gross weight of 6600 lb. Figure 3(b) combines these improvements with an improved battery of specific energy 250 Wh/kg to achieve a payload of still 1800 lb but at a slightly lower gross weight of 6200 lb at a disk loading of 10 lb/ft^2, or a payload of 1900 lb for a gross weight of 6600 lb at a disk loading of 8 lb/ft^2. Thus, it is clear that the greatest impact comes not from batteries but from the fuel cells.

Figure 3(c) shows the effects of operating at higher altitude and temperature of 5,000 ft and 20°C. The air density drops from 0.00238 to 0.00194 slugs/ft^2, and the speed of sound increases from 1116 to 1132 ft/s. As a result, the payload is reduced from 400 to 300 lb for a larger aircraft of 6500 lb weight and lower disk loading of 6.5 lb/ft^2. Altitude has a very significant impact.

Thus far, the batteries have been sized using specific energy, under the assumption that specific power (or C-rate) is not a limiting factor. Figure 3(d) shows how the payload changes if the battery is power limited. A battery's C-rate specifies ratio of its power to energy. The line for C-rating 10+ in Fig. 3(d) is the same as in Fig. 2, when power was not a limiting factor. The other lines in Fig. 3(d) show a decreasing payload due to a larger battery carrying more energy than needed to provide hover power at lower C-rates. A B–FC hybrid power plant using a 6C battery and baseline technology (150 Wh/kg battery, 0.5 kW/kg fuel cell, 5% W_f tank) is capable of carrying only a payload of 300 lb.

To summarize, the hybrid is far superior to either option alone. A 6200-lb gross-weight aircraft with a 10 lb/ft^2 disk loading, equipped with 10C lithium-ion batteries of specific energy 150 Wh/kg, a 0.5-kW/kg fuel cell stack, and 5.4% weight fraction hydrogen storage, will be capable of carrying two to three passengers. It is also shown that the technology improvements in fuel cell in general will have a more profound impact compared to improvements in batteries. With these conclusions in mind, the feasibility of actual power sharing is studied in the following sections.

Fuel Cell Test Bed

A commercial 300-W PEM fuel cell stack and a 2800-mAh three cell lithium polymer (LiPo) battery were used to construct a test bed. Due to the surrogate nature of the setup (nonflight worthy), the balance

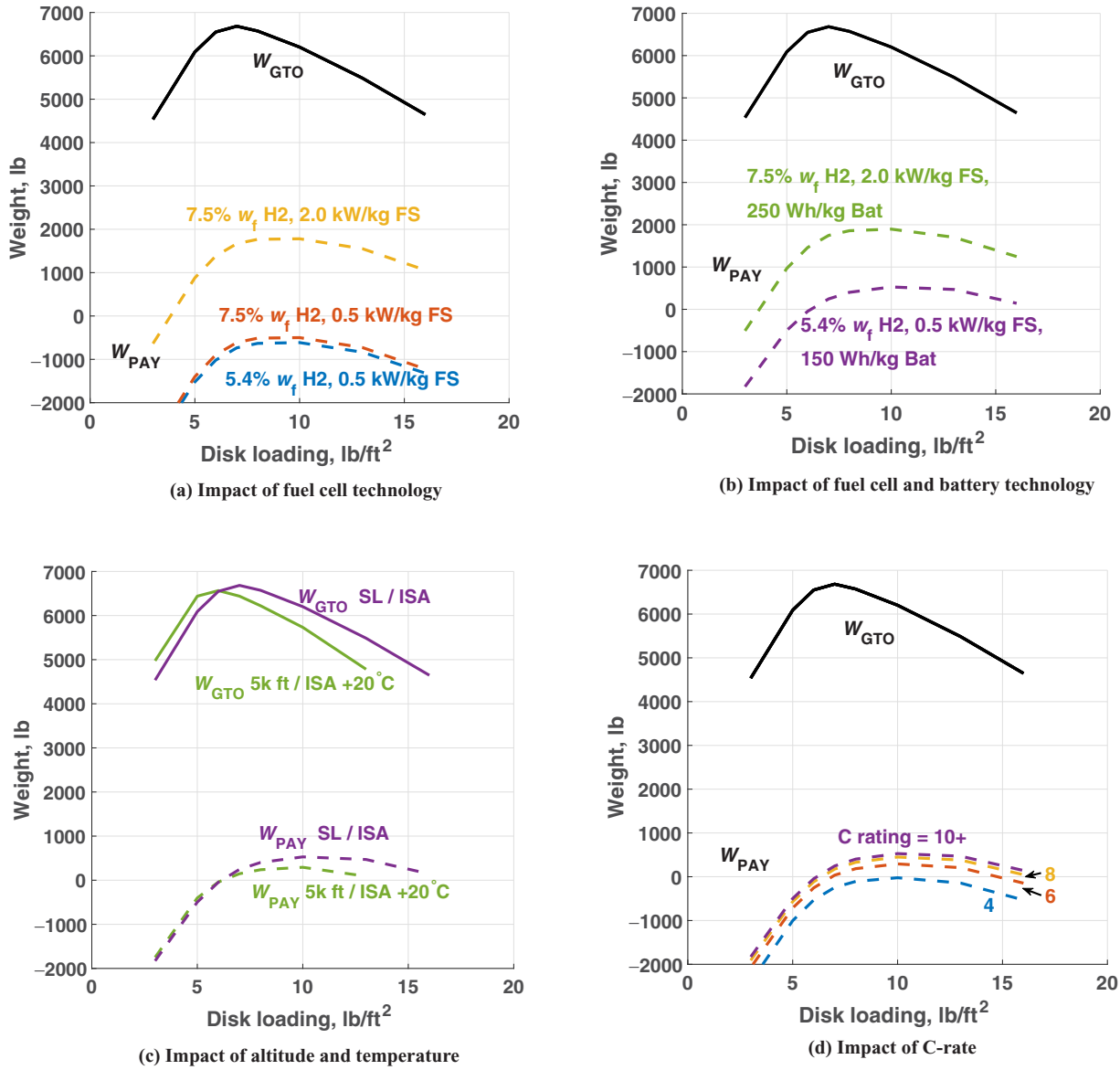

(a) Impact of fuel cell technology

(b) Impact of fuel cell and battery technology

(c) Impact of altitude and temperature

(d) Impact of C-rate

Fig. 3. Impact of key technologies and conditions on payload for a mission with 5 min hover at 500 kW and 75 miles of cruise at the best range speed: (a) impact of fuel cell technology, (b) impact of fuel cell and battery technology, (c) impact of design conditions, and (d) impact of battery C-rate.

Table 1. Component weight calibration factors.

Structure Group	Calibration Factor
Wing	1.8
Blade	1.8
Hub	0.6
Empennage	0.75
Fuselage	1.8
Alighting gear	1.2

of plant overheads—weights and power losses—are conservative. The unregulated version of power-sharing architecture is a direct connection of the two power sources in parallel with diodes. The diodes ensure the current always flows away from the sources. The regulated version adds controlled charging and discharging of the battery in a strategic manner to minimize the power plant weight. The data loggers record current and voltage over time.

A photograph of the hardware used for the baseline power plant testing is shown in Fig. 6. The fuel cell stack controller controls the supply and purge valves to allow hydrogen flow in and out of the fuel cell stack. This controller requires external power, which can be provided by a power supply or an additional battery. The fuel cell stack operates at around 50 V, so a DC–DC converter is used to reduce this voltage to that of the battery, to around 12 V. The power output from the fuel cell stack is connected in parallel with a battery. The combined power is then connected to either a bench-top programmable load or to a tethered quadcopter for flight tests.

Unregulated Architecture

The battery and the fuel cell stack are connected in parallel and power a tethered quadcopter. The data from each power source and the quadcopter load are shown in Fig. 7. The flight-test demonstrates the viability of using the two power sources together in a hybrid power plant. The

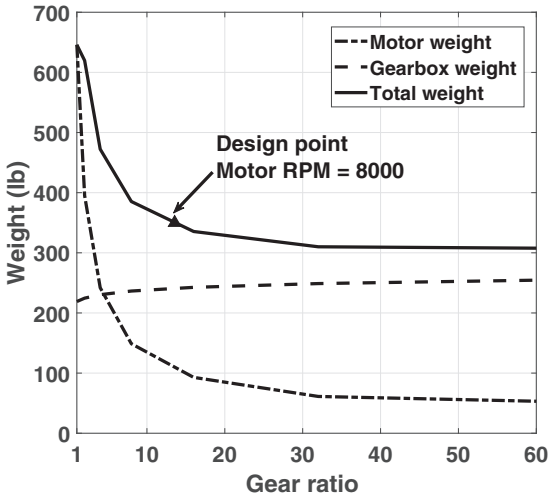

Fig. 4. Variation of motor and gearbox weight with gear ratio; motor RPM of 8000 is chosen as the design point. Gear ratio 1 is direct drive where total weight equals motor weight.

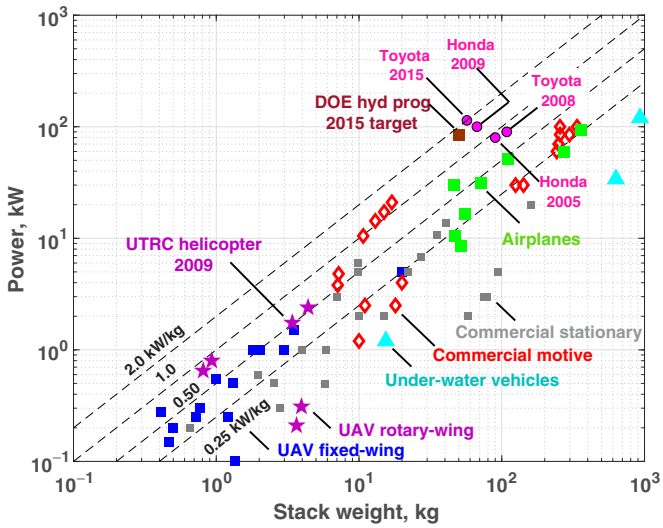

Fig. 5. State of the art in PEM fuel cell weights for power up to 100 kW. A large variation is seen across applications, and how weights are quoted.

architecture for the unregulated system is trivial (Fig. 8); the two components are connected in parallel with only diodes in series and a DC–DC step down converter in series with the fuel cell stack the same arrangement shown earlier in Fig. 6. The DC–DC step-down reduces the fuel cell stack voltage (50 V) to the order of magnitude of the battery voltage (12.3 V), and the diode prevents current flow backwards into the fuel cell stack. The power sharing is not regulated; the two components are left to operate solely on their natural voltage versus current (V–i) characteristics. The key conclusion from Fig. 7 is that they form a natural combination working in tandem—the battery voltage drops with depleting battery state of charge (soc), diminishing its share of power. This causes the fuel cell voltage to also drop, which increases its share of power, because it has different V–i characteristics from the battery. Thus, the total power supply is maintained. This is the justification for a parallel configuration, rather than a series configuration. Regulation would be required to prevent them from working in tandem, and share power as commanded. This is an essential requirement for eVTOL, where the fuel cell stack is sized to low-power cruise mode and the battery supplements during high power-segments of the mission to minimize power plant weight.

Note that the jaggedness of the fuel cell stack and battery data is due to the fuel cell stack short circuiting every 10 s—a normal mode of operation for this particular stack. The stack voltage drops to zero for 100 ms, and the battery power naturally surges to compensate. The localized drops and surges are filtered out from the raw data. However, there are some transient aftereffects, leading to the periodic jaggedness seen in the data.

This unregulated architecture will serve as a control case to compare with various regulated architectures in the next section. In addition to the quadrotor, the power plant is also connected to a programmable load. The load can be used to simulate a notional power profile, consisting of two high-power segments of hover at takeoff and landing and a low-power segment of cruise in between. These data are shown in Fig. 9. It shows a nonoptimal power-sharing behavior, where both the battery and fuel cell stack must be sized to the maximum power (exhibited at the beginning and end of the test). In the following section, a regulated architecture is developed to maintain optimal power sharing over the course of the mission.

Regulated Architecture

The regulated architecture was described in Ref. 15. Here its development is documented in a stepwise manner. A regulated architecture controls the power sharing between the two sources actively. This involves controlling the ratio of power from the two sources during the

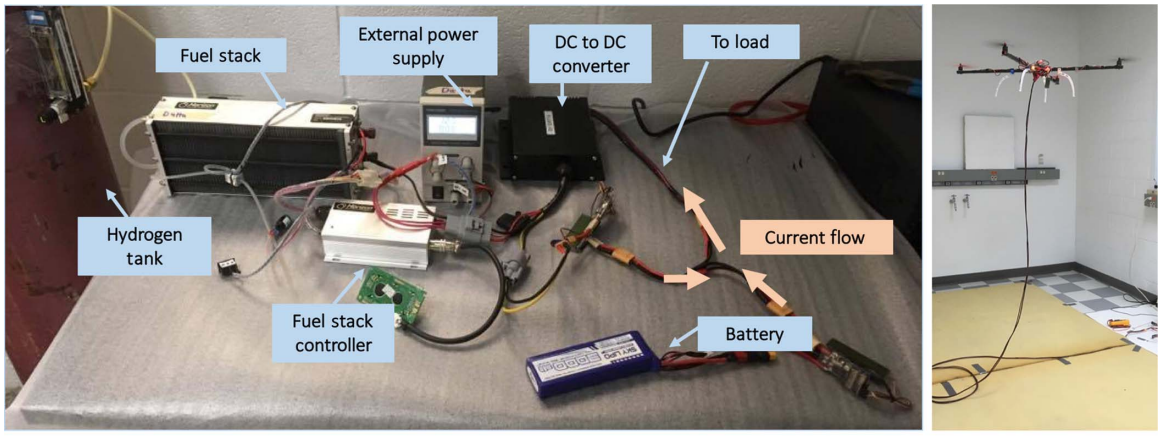

(a) Benchtop Set up (b) Tethered power

Fig. 6. Battery and fuel cell hybrid test bed: (a) setup; (b) quadcopter with tethered power.

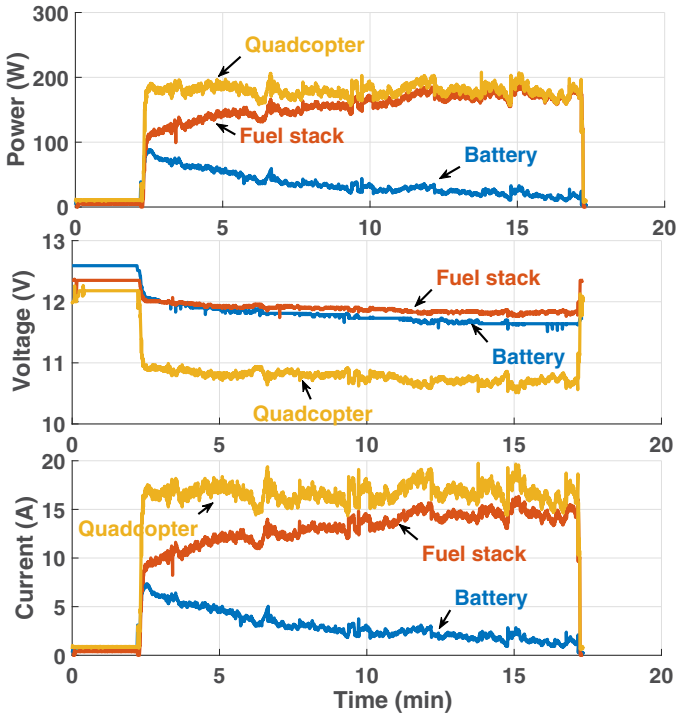

Fig. 7. Measured power, voltage, and current of battery, fuel cell stack, and quadcopter during hover: unregulated power sharing.

mission, as well as charging the battery during flight. The power diagram used by the Anteres DLR-H2 (Ref. 9) was adopted as a starting point. Improvements were made to customize it for VTOL by increasing the level of control over power sharing, and enabling high-power segment at the end of the mission.

The optimal power sharing is illustrated in Fig. 10. In designing a minimum weight power plant, the key factor is that hydrogen having higher specific energy, its weight is driven by power; whereas the battery having higher specific power, its weight is driven by energy. A regulated system would conserve battery energy and use hydrogen energy whenever possible. The battery would only be used during high-power portions of the mission to supplement the fuel cell stack, allowing the stack to be designed to a lower power and thus lower weight, and the battery to be designed to a lower energy and thus lower weight. Additionally, if the battery is depleted, any excess power from the fuel cell stack can be used to recharge it.

Baseline: Charge and discharge switches

To implement the regulated architecture, a circuit was constructed as shown in Fig. 11. The fuel cell stack and battery are still connected in parallel, but there are now two switches and two additional diodes to control charging or discharging of the battery. The switches are voltage-controlled solid-state relays activated by a microcontroller. When the relay on the left is closed, the diode in that branch limits the current flow so that the battery can only discharge. When the relay on the right is closed instead, the diode in that branch channels the current flow so that the battery can charge.

The microcontroller sets the switches open or closed depending on the battery voltage and load power. The seven operating states are described below.

State 1: The battery is fully charged, and the load power is low. All power is supplied by the fuel cell stack, and the battery is completely disconnected from the circuit. Charging is not allowed.

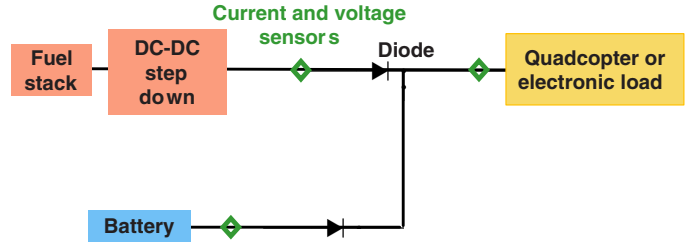

Fig. 8. Circuit schematic of unregulated configuration.

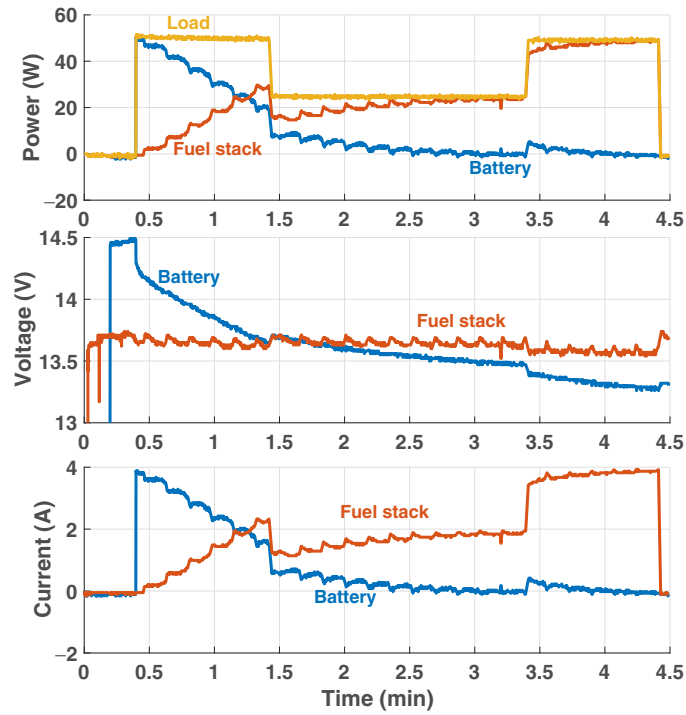

Fig. 9. Measured power, voltage, and current of battery, fuel cell stack, and controllable load during bench-top simulation of a eVTOL power profile.

State 2: The battery is fully charged, and the load power is higher than what can be supplied by the fuel cell stack alone. The battery discharge switch is closed, allowing the battery to share the load with the fuel cell stack.

State 3: The battery is depleted, but still above its safe minimum voltage. The load power is low. The battery is prevented from discharging. The fuel cell stack provides all power to the load and uses any excess power available to charge the battery.

State 4: The battery is in State 3, but the load power is higher than what can be supplied by the fuel cell stack alone. The battery discharge switch is closed, allowing the battery to share the load with the fuel cell stack.

State 5: The battery is completely depleted. The load power is low. The battery discharge switch is open, so it cannot provide power to the load. The fuel cell stack provides all the power to the load and uses any excess power available to charge the battery.

State 6: The battery is completely depleted, but the load power is above the maximum fuel cell stack power. The fuel cell stack cannot charge the battery because the load demands all of its power

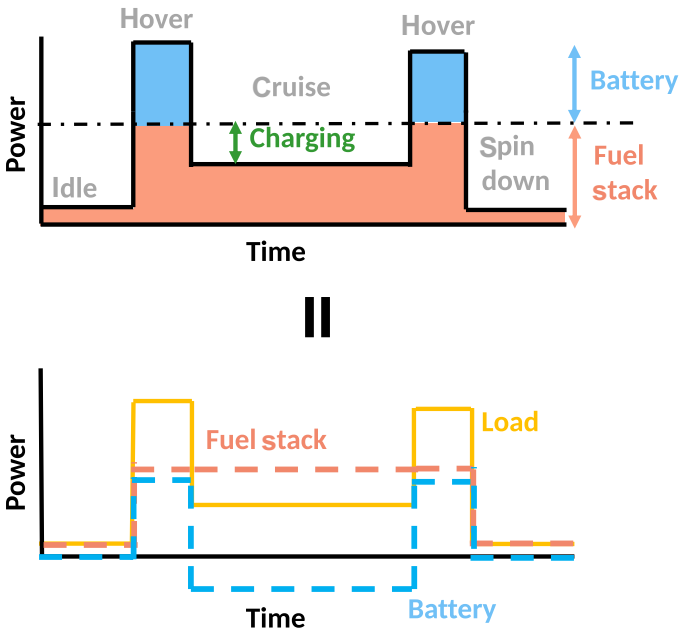

Fig. 10. Power supplied by fuel cell stack and battery in regulated operation for a notional mission power profile.

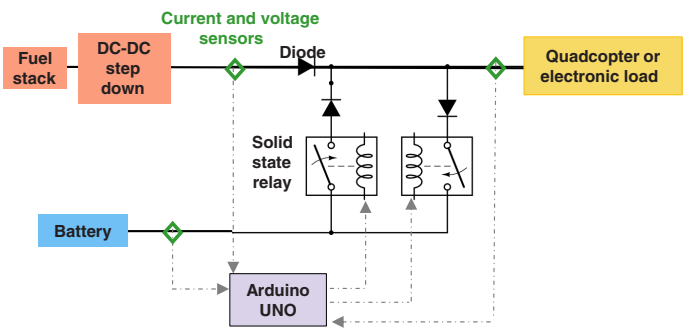

Fig. 11. Circuit schematic for regulated power sharing operation.

and more. If this case is ever reached, the battery was not sized adequately.

State 7: If the battery charge or discharge current exceeds the maximum rated current, both switches open to disconnect it from the circuit as a safety precaution.

Experimental demonstration of these individual states can be found in Ref. 15. Here, the focus is on the eVTOL power profile. The notional power profile was placed on this circuit, and the results are shown in Fig. 12. This shows an improvement from the unregulated architecture. The battery is now turned off during the low-power segment, conserving energy. The fuel cell stack is operating at its design power, and expending hydrogen, the comparatively lightweight energy source. This makes the overall system lighter. However, the desired charging of the battery is not observed. This is because the battery voltage is still higher than the fuel cell stack voltage, as seen in the bottom plot of Fig. 12, so there is insufficient voltage potential to charge the battery. Additionally, the power sharing ratio is not held constant as desired. Initially, the battery is providing all the power, which means battery energy is being consumed when it is not needed, and the fuel cell stack is not operating at its maximum design power. Then, toward the end of the test, the fuel cell stack is providing all the power, which means fuel cell stack would have to be much heavier.

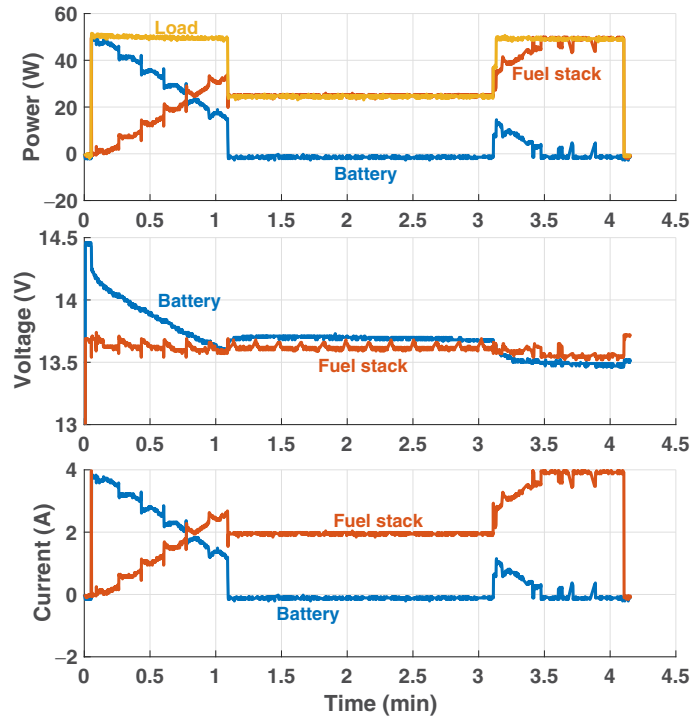

Fig. 12. Measured power, voltage, and current of battery and fuel cell stack in a regulated parallel configuration for a notional eVTOL mission with switches to control charging and discharging.

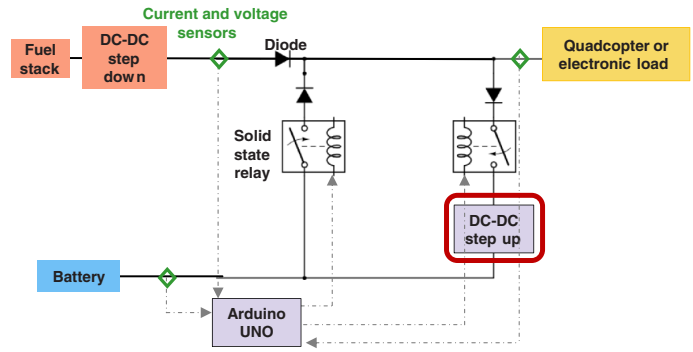

Fig. 13. Circuit schematic for regulated power-sharing operation with added DC–DC converter for constant current charging.

Refinement 1: Constant current charging

To address the inability to charge, a DC–DC step-up converter was incorporated into the charging branch of the circuit, as shown in Fig. 13. It increases the voltage across the battery to ensure a constant current (set by the user using a potentiometer) is delivered to charge the battery. The data are shown in Fig. 14. It is clear that the fuel cell stack is charging the battery in the low-power segment, as indicated by the negative battery power and increasing battery voltage, but the power sharing ratio is still not constant.

Refinement 2: Constant voltage discharge

To address the problem above, a DC–DC step-down (buck-boost) converter was incorporated into the discharging branch of the circuit,

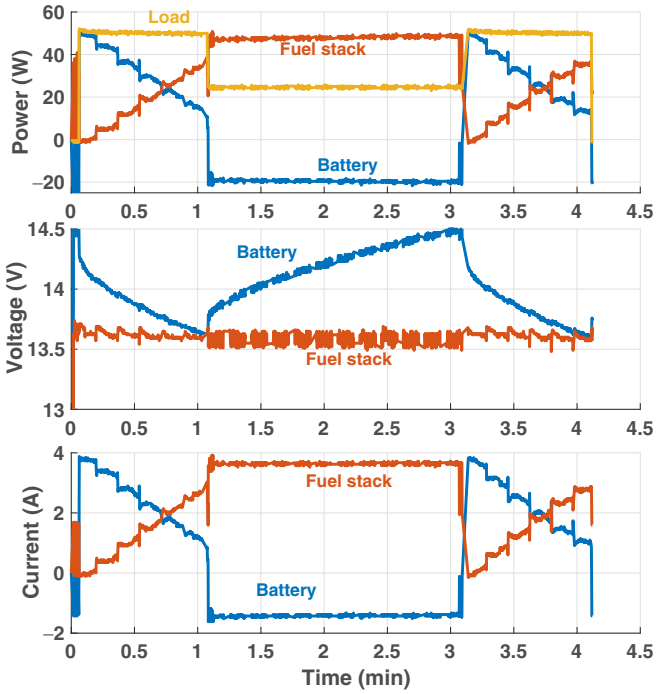

Fig. 14. Measured power, voltage, and current of battery and fuel cell stack in a regulated parallel configuration for a notional eVTOL mission with added DC–DC converter for constant current charging.

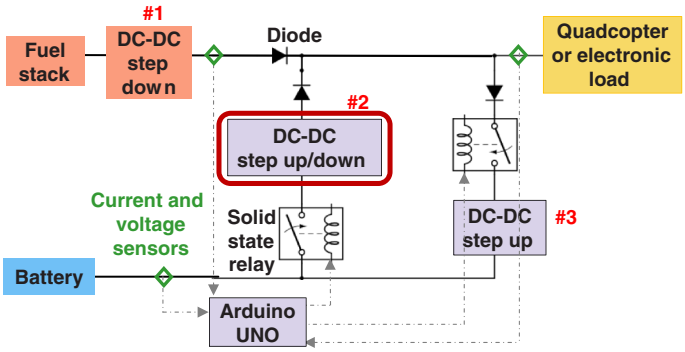

Fig. 15. Circuit schematic for regulated power sharing operation with added DC–DC converter for constant voltage discharging.

as shown in Fig. 15. This component allows the user to set a constant voltage for the battery power, regardless of the battery voltage. The data are shown in Fig. 16.

This circuit almost achieves the ideal power sharing scenario in Fig. 10. The remaining difference is that the fuel cell stack power contribution is not constant over the course of the mission. The fuel cell stack is still not operating at its full power during hover, forcing the battery to supplement more power than necessary. This cannot be corrected by changing the circuit, but only by redesigning the fuel cell stack and battery to fit this specific mission. A power plant sized to mission would have a reduced capacity battery set to a lower discharge voltage by the DC–DC converter, which would increase the fuel cell stack power during hover. The smaller battery can then be charged at a lower current during cruise, which would reduce the fuel cell stack power during cruise, and thus reduce the design power of the stack. The lower capacity battery and lower power stack would both lead to reductions in the power plant weight.

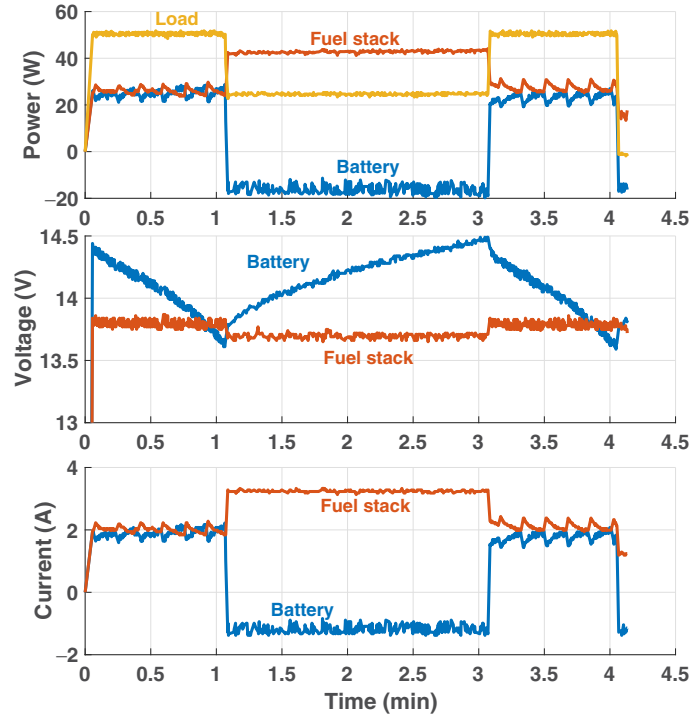

Fig. 16. Measured power, voltage, and current of battery and fuel cell stack in a regulated parallel configuration for a notional eVTOL mission; DC–DC converter added for constant voltage discharging.

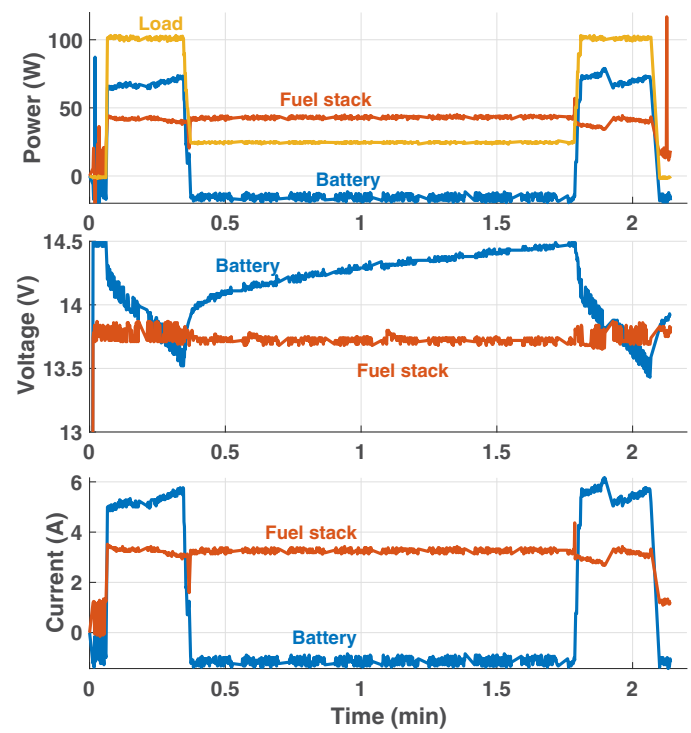

Fig. 17. Measured power, voltage, and current of battery and fuel cell stack in regulated parallel configuration for a notional eVTOL mission: with final architecture.

The fuel cell stack and battery design power, P_f and P_b, can be calculated for a given high-power P_{hi} (segment of time t_{hi} representing hover), a low-power P_{lo} (segment of time t_{lo} representing cruise) by

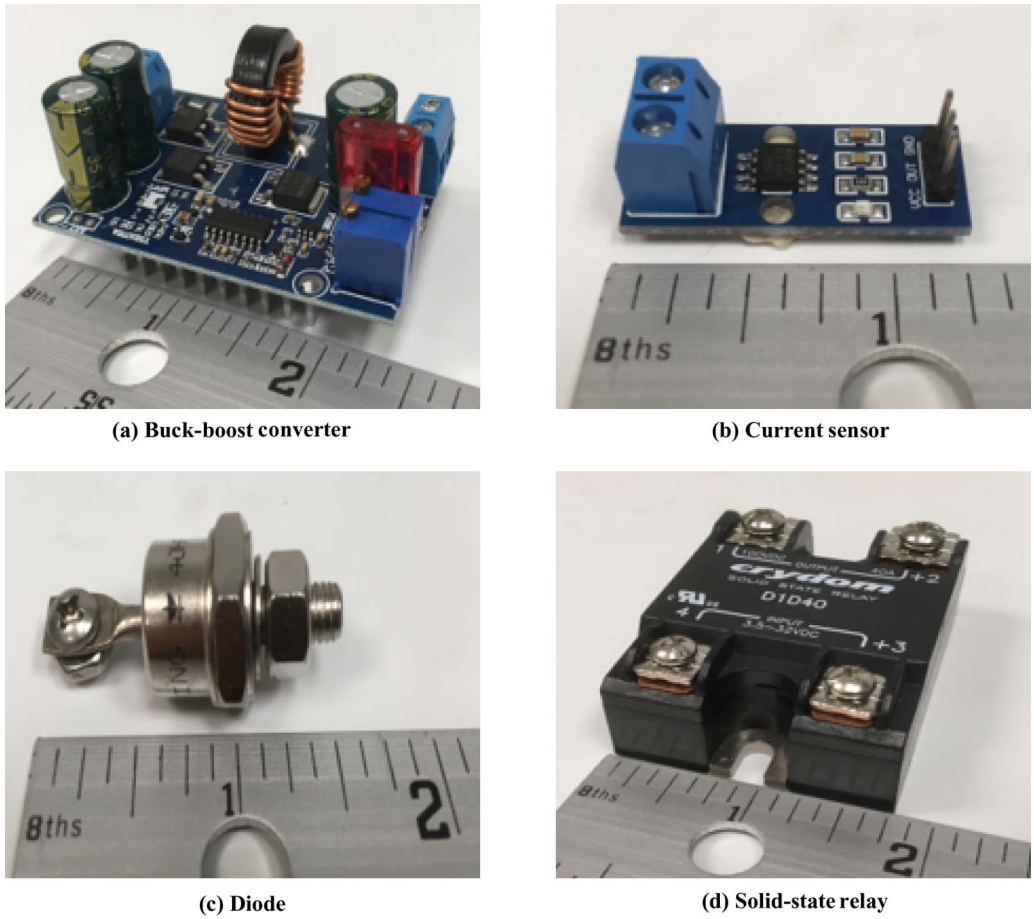

(a) Buck-boost converter (b) Current sensor

(c) Diode (d) Solid-state relay

Fig. 18. Power electronic components used for regulation. (a) Buck-boost converter: 5–32 V to 1.25–20 V DC converter, 60 W power rating, by DROK; (b) current sensor: 30 A measurement range, 5 V working voltage, ACS712 chip Hall sensor module, by SMAKN; (c) blocking diode: NTE5991 silicon power rectifier diode, 40 amp current rating, 400 V, by NTE Electronics; (d) relay : D1D40 solid state relay, 3.5–32 VDC input, 0–100 V load voltage, 40 A load current, by Sensata-Crydom.

solving the two equations given below:

$$\begin{aligned} P_{hi} &= P_f + P_b \\ (P_f - P_b)t_{lo} &= E_b \end{aligned} \tag{1}$$

Here, $E_b = P_b t_{hi}/2$ is the total energy required from the battery in each high power segment (two equal segments assumed here). If no charging is assumed on the fly, $E_b = P_b t_{hi}$. Resizing the power plant is beyond the scope of this setup, as it would require purchasing a new, custom-made fuel cell stack, but is also not necessary. Instead, an ideal power profile can be found for the existing power plant. This profile is used to demonstrate ideal power sharing in Fig. 17. In summary: (1) the fuel cell stack operates at a constant power, (2) the battery supplements during high-load portions of the mission, (3) a user-defined constant ratio of battery and fuel cell stack power sharing is maintained, and (4) the fuel cell stack is used to charge the battery during low-load portions. This minimizes the design power of the fuel cell stack and the design energy of the battery. Thus, the hybridization concept used earlier in the eVTOL Sizing section is proved to be possible.

The overhead incurred in weight and power are as follows: Each of the two DC–DC converters causes an efficiency loss of around 10%. The mass of the two DC–DC converters is 41 g. The DC–DC step-down after the fuel cell stack is not considered part of the architecture. If properly designed, with similar voltage ranges—this step-down converter would not be needed.

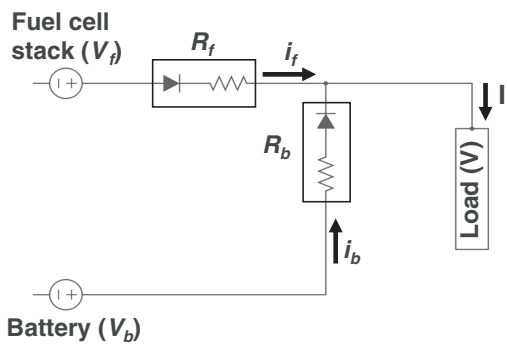

Fig. 19. Simplest representation of power-sharing circuit.

Regulators and sensors

The key components selected for this regulated architecture are shown in Fig. 18. The buck/boost (step-up/-down) converter is set manually using two potentiometers to deliver a constant current or constant voltage. The hall current sensors were selected because they measure current in both directions. The blocking diode was selected over other diodes due it its ability to withstand high currents and voltages. The solid-state relay was chosen over other switching mechanisms due to its reliability.

Power Plant Modeling

The circuit shown earlier in Fig. 15 is capable of achieving regulated power sharing between battery and fuel cell stack with the help of relays, diodes, and DC–DC converters. The objective in this section is to model this circuit.

Circuit parameters

Figure 19 shows the simplest representation of a power-sharing circuit. This circuit comprises active components battery and fuel cell stack and passive components load, diodes, and resistance of wires. The diodes ensure unidirectional passage of current from active sources to the load.

The notations V_b, V_f, and V denote the voltages of the battery, fuel cell stack, and load, respectively. The notations i_b, i_f, and I represent the currents flowing from/into the battery, the fuel stack, and the load, respectively. The resistance in the two branches are lumped as R_b and R_f, respectively. Because diodes are semiconductor devices doped with impurities, they do not function like linear devices. Their resistance changes with voltage and current given by

$$R = f(V, i) = k \quad i^e \tag{2}$$

where k and e are constants determined from calibration.

The power-sharing ratio is represented by α, defined—as the fraction of battery power to total power,

$$\alpha = \frac{P_b}{P_b + P_f} \tag{3}$$

where

$$P_b = V_b i_b \quad \text{and} \quad P_f = V_f i_f \tag{4}$$

The heat dissipated in the resistance is accounted for using a parameter κ—which denotes the ratio of load power to the generated power,

$$\kappa = \frac{P}{P_b + P_f} \tag{5}$$

In an ideal case of perfectly conducting wires $\kappa = 1$, implying the load power is equal to generated power. The value of κ in our test bed ranges from 0.90 to 0.95.

Circuit operation

For a permanent magnet motor, the torque is proportional to the current and the RPM is proportional to voltage. So the torque and RPM profile nominally represents the current and voltage, respectively. Understanding the circuit operation is critical in modeling the circuit. A brief explanation on the working of the circuit is presented below.

Discharging segment. Consider the case when the battery is discharging. Figure 20(a) shows notional voltage–current (V–i) operating curves for the fuel cell stack and the battery. Consider point P to be the initial point of operation with both battery and fuel cell stack contributing equally to

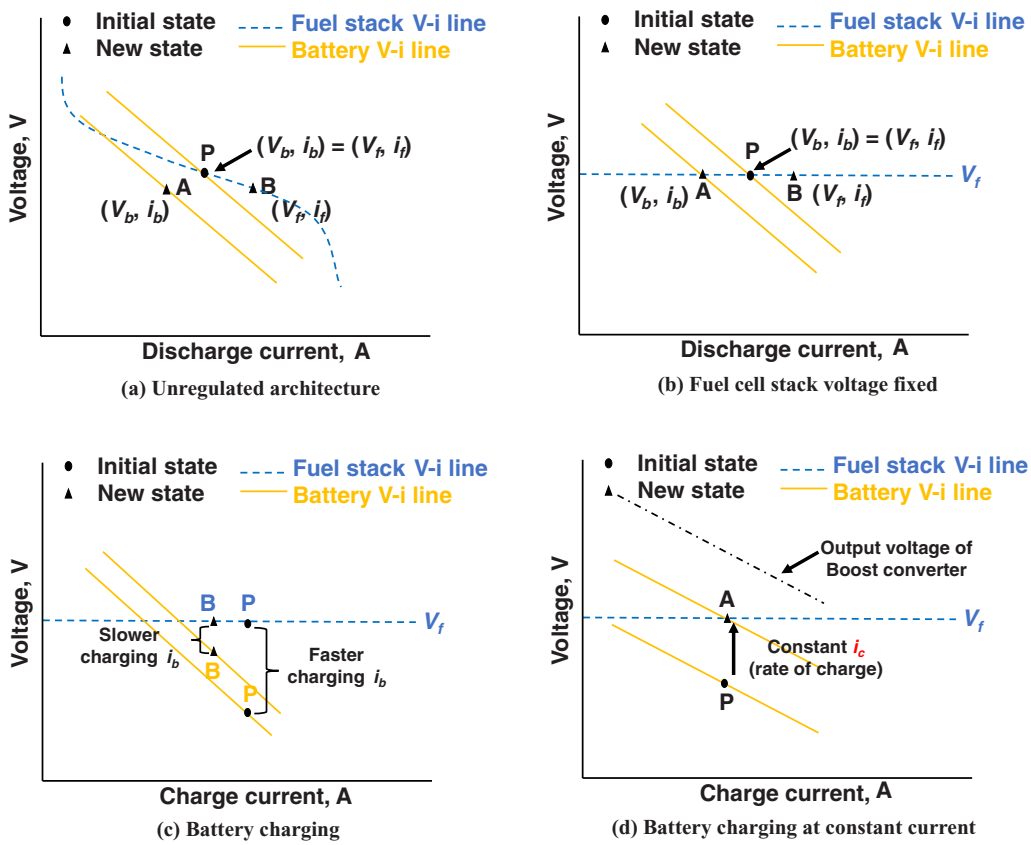

(a) Unregulated architecture

(b) Fuel cell stack voltage fixed

(c) Battery charging

(d) Battery charging at constant current

Fig. 20. Illustration of circuit operation (a) along natural *V–i* lines with no converters; (b) with a DC–DC converter added in series with the fuel cell stack to produce a flat output voltage; (c) with battery charging without boost converter—charging current decreases with state of charge; (d) with battery charging with a boost converter—charging current remains constant.

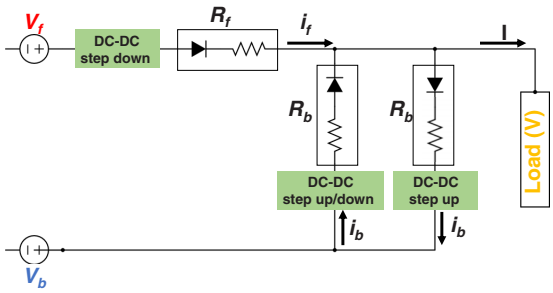

Fig. 21. Circuit diagram of regulated power-sharing operation.

the load. As the battery discharges, the decreasing state of charge drops its open-circuit voltage and shifts the operating curve down. The voltage V_b must still equal V_f as they are connected in parallel. So the circuit will naturally find the voltage for which the total load current still supplies the load power. This voltage must be lower in order for the total load current to remain the same as before. The battery now supplies a lower current (point A in Fig. 20(a)). The fuel cell stack now supplies a higher current (point B in Fig. 20(a)).

In general, the V–i characteristics of two components need not intersect; they might be parallel, or more likely one operating at a higher voltage than the other. It is desirable therefore to have a DC–DC converter in series with at least one of the two components to produce a flat output voltage. In the present test bed, the fuel cell stack operates at a higher voltage, so it is the fuel cell stack that is fitted with the buck (step-down) converter. This is shown in Fig. 20(b). Now, as the battery operating curve shifts down, the voltage remains the same, only the current supply drops. And because the load current must also remain the same, the stack current must increase (point B in Fig. 20(b)). These explain the self-equilibrating conditions seen earlier in the unregulated architecture (Figs. 8 and 9).

The contribution from the battery α decreases continuously in the unregulated architecture. To overcome the problem of varying α with time, a buck-boost (step-up/-down) converter is used in the battery discharge branch (marked as 2 in Fig. 15). This converter steps up or down the battery voltage to a target voltage preset by the user for achieving a desired α. The contribution from the battery then is solely dependent on the output voltage of the converter. As a result, any battery can successfully complete the mission as long as it operates within its limits—i_b does not exceed the maximum allowable current, and V_b does not fall below the minimum allowable voltage.

Charging segment. Now consider the case when the battery is charging. To implement this option, a third line is needed from the fuel cell stack to the battery. The fuel cell stack can then be allowed to charge the battery when V_b falls below a certain threshold.

Provisions must be made for constant current charging. The current is determined by the voltage difference between the fuel cell stack and the battery. As the battery charges, its state of charge increases and the difference between V_b and V_f diminishes (point B in Fig. 20(c)). To ensure a constant current charging, a boost (step-up) converter is used in the third line (marked as 3 in Fig. 15). The output current from the boost converter can be preset by the user. This current i_c represents the charging rate of the battery. Then, the output voltage of the converter is allowed to vary such that the output current is constant. Figure 20(d) gives a pictorial illustration. The final circuit is shown in Fig. 21. It is the mathematical model of the circuit in Fig. 15.

Governing equations

The governing equations for modeling the circuit are determined from Kirchhoff's circuit laws of current and voltage balance. Current balance gives

$$i_b + i_f = I \tag{6}$$

Voltage balance over two branches give

$$V_b(i_b, soc) - i_b R_b = V \tag{7}$$

$$V_f - i_f R_f = V \tag{8}$$

The power-sharing ratio, α, gives the additional relation:

$$V_b i_b - \alpha(V_b i_b + V_f i_f) = 0 \tag{9}$$

Equations (6)–(9) form the governing equations of the circuit. The resistances R_b ($k = 0.7429$, $e = 0.949$) and R_f ($k = 0.7518$, $e = 0.947$) are functions of current because of the diodes (Eq. (2)), so these are nonlinear equations to be solved iteratively. It is important to enforce zero as a lower bound otherwise negative nonphysical values are possible. There are three possible tasks:

1) **Given** : V_b, V_f, I **Find** : i_b, i_f, V, α
2) **Given** : V, I, α **Find** : V_b, V_f, i_b, i_f
3) **Given** : V_b or V_f, I, V **Find** : V_f or V_b, i_b, i_f, α

Modeling of DC–DC converters. There are three DC–DC converters (Fig. 15). The effect of these converters is modeled using conservation of power. For example, consider the branch which has the step-up/down converter—with V_b and i_b as its inputs and—V_c and i_c as outputs. One can write

$$V_b i_b = \beta \quad V_c i_c \tag{10}$$

where β is the fraction of input to output power. β is obtained by calibrating the converter separately ($\beta = 1.10$ for all converters). In the case of step-up/down converter and the step-down converter, V_c is set by the user. In the case of the step-up converter, i_c is set by the user.

Transient operation. All the three tasks mentioned above can be used for obtaining transient states. For illustration, task 2 is chosen here. During the transient operation, $V(t)$ and $I(t)$ are known (possibly deduced from motor RPM and torque). For any desired power sharing ratio α, the task is to calculate the battery and fuel stack voltages and the currents. In summary:

Given : $V(t)$, $I(t)$, α

Find : $V_b(t)$, $V_f(t)$, $i_b(t)$, $i_f(t)$.

The solution procedure begins by solving the equations for V_{bo}, V_{fo}, i_{bo}, i_{fo} based on the maximum power requirement obtained from V and I. These determine the specifications of the battery and fuel cell stack required to complete the mission. For example, consider a mission with a maximum required power of 100 W ($V = 20$ V, I = 5 A), and desired $\alpha = 0.3$—solving the equations result in $V_{bo} = 20.75$ V, $V_{fo} = 20.8$ V, $i_{bo} = 1.5$ A, $i_{fo} = 3.5$ A—implying that a battery with a minimum starting voltage of V_{bo} is required to supply the desired power. In a similar manner, these equations are now solved at each time-step to obtain the transient response. The output voltages of step-up/down converter and step-up converter (V_c) are set to V_{bo} and V_{fo}, respectively. The output currents of step-up/down converter and step-up converter (i_c) therefore

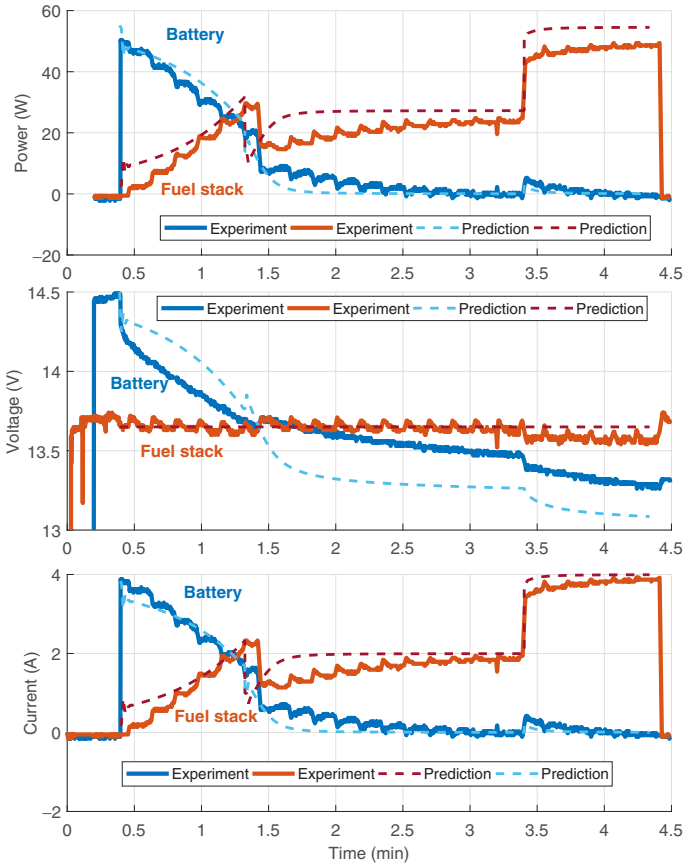

Fig. 22. Validation of results with test data for unregulated architecture.

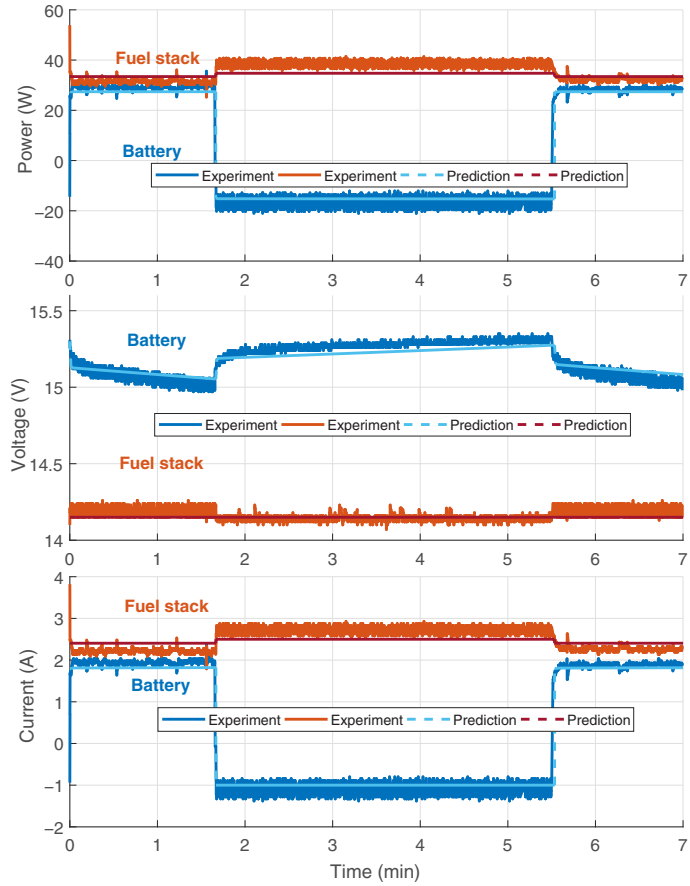

Fig. 23. Validation of results with test data for regulated architecture.

become i_{bo} and i_{fo}, respectively. These initial settings will ensure the desired power-sharing ratio. The transient states of the battery and fuel cell stack are obtained as follows. For each time step:

1) Using Eq. (10), compute i_b (current flowing from battery)

2) Compute the new state of charge of the battery using

$$soc(t) = soc_o - \frac{1}{C}\int_0^t i_b \, d\tau \tag{11}$$

where soc_o is the initial state of charge of the battery, C is its total capacity (in Ah), and t (in hours) is the time elapsed from start.

3) Calculate V_b from soc using Eq. (13).

$$V_b = E_r - i_b N \tag{12}$$

where

$$E_r = E_s - \frac{K}{soc} i_b + A \exp\left[-B(1 - soc)\right] \tag{13}$$

This is a semiempirical model of battery voltage as a function of current draw i_b and battery state of charge soc and is explained in detail in Ref. 15. The constants are calibrated for the battery using empirical data—$E_s = 14.7$ V, $K = 0.004\ \Omega$, $N = 0.079\ \Omega$, $A = 2.2$, V, and $B = 2.3$. Reference 15 gives more refined models for Eq. (13), which can be used instead of the simple linear model shown here. The refined models are important for rapid transients.

4) Proceed to next time step.

At every time step, check for $V_b > (V_b)_{\min}$ and $i_b < (i_b)_{\max}$. If false, battery can no longer be used for discharging until further charged. During the charging segment, the governing equations are still valid and above steps are repeated with a negative i_b.

Validation of model

The above model was used to predict the dynamics of battery and fuel cell stack for two cases, namely, unregulated and regulated architecture. Figures 22 and 23 show the variation of V_b, V_f, i_b, and i_f for a generalized mission profile obtained using the test and model for unregulated and regulated architecture, respectively. In case of the unregulated architecture, the predicted results from the model are in good agreement with the test data for all parameters except the battery voltage. This is perhaps because the tests were performed with the battery at a low state of charge. In case of regulated, the predicted results from the model are in good agreement with the experimental data.

Conclusions

This paper demonstrated ideal power sharing between hydrogen fuel cells and lithium-ion batteries suitable for eVTOL–like power profiles. The benefits of combining the two sources was first demonstrated on paper by conceptual sizing of an electric tiltrotor. Next, the operation of a parallel B–FC system was explored using testing and simulation. Unregulated and regulated power-sharing architectures were developed and tested. A regulated architecture necessary and sufficient to achieve ideal power sharing was built up in a step-by-step manner. A power system model was developed, and data from the test bed was used to validate

the model and gain fundamental understanding of the power sharing architecture. Based on these studies, the following key conclusions are drawn:

1) Power sharing between a battery and fuel cell stack can indeed be regulated in a manner that minimizes the power plant weight. Here, the fuel cell stack supplies a constant nominal power, the battery supplements during high-power segments of the mission, and the fuel cell stack charges the battery during low-power segments of the mission.

2) Power regulation can be accomplished using two switches and three DC–DC converters. The two switches control charging and discharging of the battery. They are voltage-controlled solid-state relays. The DC–DC converters each has a special purpose. Converter 1 is required to ensure the same parallel bus voltage is maintained given that the two components will have a different current–voltage behavior and in general produce two different voltages. If a custom-designed fuel cell stack and battery were used, with similar voltage ranges, this converter would not be necessary at all. Converter 2 is required to enforce constant-current charging of the battery regardless of its state of charge. Converter 3 is required to compensate for the continuous drop in battery voltage due to depleting state of charge and enforce constant power discharge.

3) Overall there are six key operating states of regulated power sharing—the seventh is a safety shutdown. A controller executes the circuit branches to implement these states. These are driven by the battery state of the charge: high (fresh battery), medium (nominal), and low (nearing discharge)—designated by the designer. Corresponding to each state, there is a pair of loading scenarios: low and high. These scenarios are driven by current required at the load.

4) If executed in the ideal power-sharing mode, the impact of B–FC hybrid power system can be dramatic. For an example mission of 75 miles and 5 min hover, an electric tiltrotor with a B–FC hybrid power plant is far superior to either option alone. This study indicates that a 6200-lb gross-weight aircraft with a 10-lb/ft^2 disk loading, equipped with state-of the art 10C lithium-ion batteries of specific energy 150 Wh/kg, a 0.5-kW/kg fuel cell stack, and 5% weight fraction storage, will be capable of carrying a 500-lb payload (at least two passengers).

5) With near-future technology, some of which are already being reported by industry at a component level—2 kW/kg for fuel cells, 7.5% weight fraction hydrogen storage, and 250 Wh/kg pack level—the same mission can be flown with an aircraft of a gross takeoff weight of 6200 lb but carrying a payload of 1800 lb. The impact on payload is primarily driven by improvements in the fuel cell stack, not batteries. A fuel cell-only power plant can itself produce the same benefit.

Acknowledgments

This work is carried out at the Alfred Gessow Rotorcraft Center, University of Maryland at College Park, under the Army/Navy/NASA Vertical Lift Research Center of Excellence (VLRCOE) grant (number W911W61120012), with technical monitoring from Dr. Mahendra Bhagwat and Dr. William Lewis. Additional funding for test hardware was provided by Army Research Laboratories, with technical monitoring from Dr. Rajneesh Singh. We wish to thank Dr. Josef Kallo (DLR and University of Ulm) for his insights. We also thank undergraduate intern Mr. Faran Masood for building and flying the quadrotor.

References

[1]Colucci, F., "Lift Where You Need It," *Vertiflite*, Vol. 62, (6), November–December 2016, pp. 26–30.

[2]Whittle, R., "Air Mobility Bonanza Beckons Electric VTOL Developers," *Vertiflite*, Vol. 63, (2), March–April 2017, pp. 14–21.

[3]Chretien, P., "The Quest for the World's First Electric Manned Helicopter Flight," *Vertiflite*, Vol. 58, (2), March–April 2012, pp. 38–42.

[4]Schneider, D., "Helicopters Go Electric," *IEEE Spectrum*, Vol. 49, (1), January 2012, pp. 11–12.

[5]Holden, J., and Goel, N., "Fast-Forwarding to a Future of On-Demand Urban Air Transportation," *UBER Elevate*, October 2016.

[6]Lapeña-Rey, N., Mosquera, J., Bataller, E., and Ortí, F., "First Fuel-Cell Manned Aircraft," *Journal of Aircraft*, Vol. 47, (6), November 2010, pp. 1825–1835.

[7]Rathke, P., Kallo, J., Schirmer, J., Stephan, T., Waiblinger, W., and Weiss-Ungethüm, J., "Antares DLR-H2 Flying Test Bed for Development of Aircraft Fuel Cell Systems," *ECS Transactions*, Vol. 51, (1), June 2013, pp. 229–241.

[8]Flade, S., Kallo, J., Schirmer, J., and Stephan, T., "Comparison of Anode Configurations during Long Distance Flight in Fuel Cell Powered Aircraft Antares DLR-H2," Proceedings of the AIAA SciTech Forum 52nd Aerospace Sciences Meeting, National Harbor, MD, January 13–17, 2014.

[9]Kallo, J., Flade, S., Stephan, T., and Schirmer, J., "Antares DLR H2—Test Bed for Electric Propulsion," Proceedings of the 53rd AIAA Aerospace Sciences Meeting, Kissimmee, FL, January 5-9, 2015.

[10]Romeo, G., Borello, F., Correa, G., and Cestino, E., "ENFICA-FC: Design of Transport Aircraft Powered by Fuel Cell & Flight Test of Zero Emission 2-Seater Aircraft Powered by Fuel Cells Fueled by Hydrogen," *International Journal of Hydrogen Energy*, Vol. 38, (1), January 2013, pp. 469–479.

[11]Moffitt, B. A., and Zaffou, R., "Polymer-Electrolyte Fuel Cells for UAV Applications Providing Solutions to Revolutionize UAVs," *SAE Technical Papers*, Vol. 10, October 2012, SAE International, Warrendale, PA.

[12]EnergyOr Shows Off World's First Fuel Cell Multirotor UAV. *Fuel Cells Bulletin*, Vol. 2015, (4), April 2015, pp. 5–6.

[13]Datta, A., and Johnson, W., "Requirements for a Hydrogen Powered All-Electric Manned Helicopter," AIAA 2012-5405, Proceedings of the 12th AIAA ATIO Conference, Indianapolis, IN, September 12–17, 2012.

[14]Datta, A., and Johnson, W., "Powerplant Design and Performance Analysis of a Manned All-Electric Helicopter," *Journal of Propulsion and Power*, Vol. 30, (2), February 2014, pp. 490–505.

[15]Ng, W., and Datta, A., "Hydrogen Fuel Cells and Batteries for Electric-Vertical Takeoff and Landing Aircraft," *Journal of Aircraft*, Vol. 56, (5), September 2019, pp. 1765–1782.

[16]Ng, W., Patil, M., and Datta, A., "Hydrogen Fuel Cell and Battery Hybrid Architecture for Range Extension of Electric VTOL (eVTOL) Aircraft," Proceedings of the 75th Annual Forum of the Vertical Flight Society, Philadelphia, PA, May 13–16, 2019.

[17]Johnson, W., "NDARC-NASA Design and Analysis of Rotorcraft Validation and Demonstration," Proceedings of the AHS Aeromechanics Specialists Conference, San Francisco, CA, January 20–22, 2010.

[18]Matsunaga, M., Fukushima, T., and Ojima, K., "Powertrain System of Honda FCX Clarity Fuel Cell Vehicle," *World Electric Vehicle Journal*, Vol. 3, (4), December 2009, pp. 820–829.

[19]Yoshida, T., and Kojima, K., "Toyota MIRAI Fuel Cell Vehicle and Progress Toward a Future Hydrogen Society," *The Electrochemical Society Interface*, Vol. 24, (2), January 2015, pp. 45–49.

[20]Hasegawa, T., Imanishi, H., Nada, M., and Ikogi, Y., "Development of the Fuel Cell System in the Mirai FCV," SAE Technical Paper 2016-01-1185, Proceedings of the SAE 2016 World Congress and Exhibition, Detroit, MI, April 2016.